Bellis et al., http://www.jcb.org/cgi/content/full/jcb.201204086/DC1

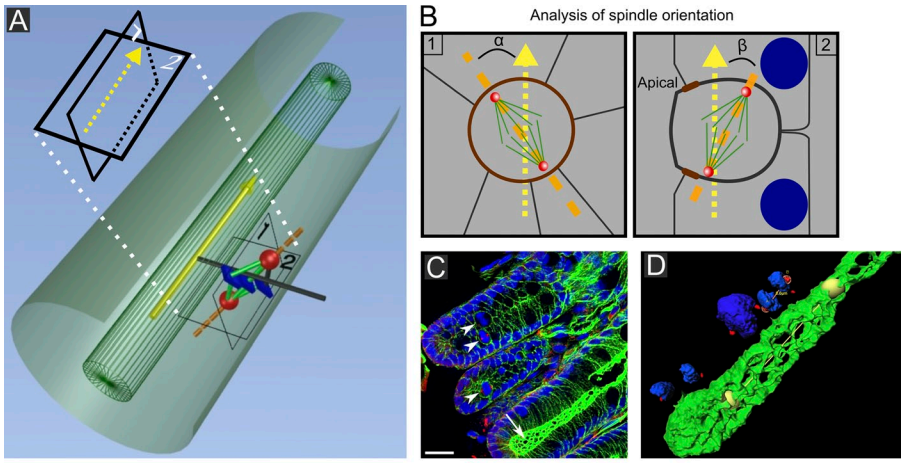

E α angle

	mean	sd	p-value	n
$Apc^{+/+}$	20	18		67
$Apc^{\Delta 14/+}$	23	21	0.42	45
$Apc^{1638N/+}$	26	19	0.13	52
$Apc^{Min/+}$ small intestine	23	18	0.52	45
$Apc^{Min/+}$ colon	24	21	0.36	47
$Apc^{\Delta 14/-}$ ACF	34	25	0.001*	47
$Apc^{-/-}$	44	24	0.001*	17

F β angle

	mean	sd	p-value
$Apc^{+/+}$	7	5	
$Apc^{\Delta 14/+}$	8	8	0.54
$Apc^{1638N/+}$	9	7	0.28
$Apc^{Min/+}$ small intestine	9	8	0.16
$Apc^{Min/+}$ colon	8	9	0.48
$Apc^{\Delta 14/-}$ ACF	8	6	0.7
$Apc^{-/-}$	17	11	0.003*

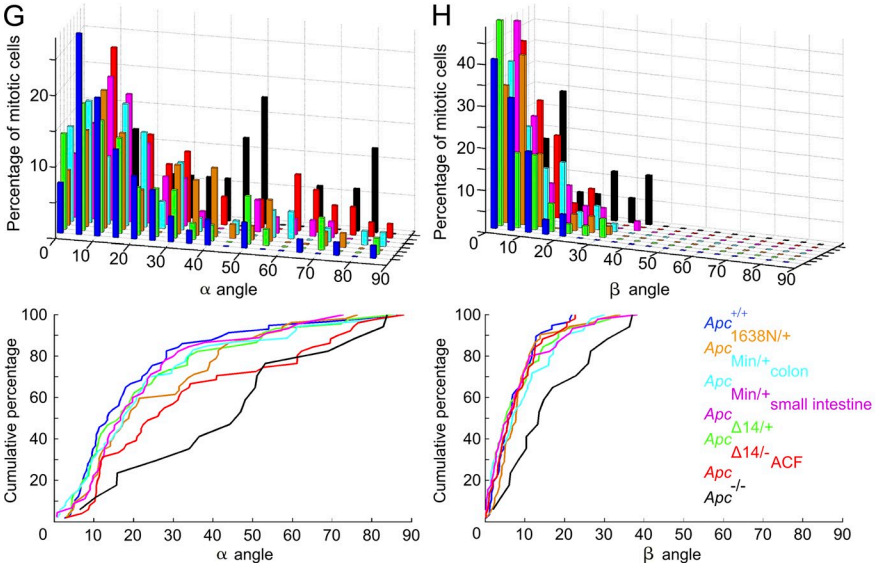

Figure S1. **Imaging of intact colon crypts and analysis of spindle orientation by measuring angles α and β in wt and *Apc* mutant mice shows normal OCD in crypts from $Apc^{1638N/+}$, $Apc^{Min/+}$, and $Apc^{\Delta 14/+}$ mice but perturbation upon sudden loss of *Apc* in crypts of floxed *Apc* × *Villin-CreERT2* mice treated with tamoxifen, isolated 5 d after tamoxifen administration, and upon LOH in ACF of $Apc^{\Delta 14/+}$ mice.** (A) Diagram of a metaphase spindle within a crypt and the reference planes used to determine the two angles α and β. Plane 1 is perpendicular to the gray line passing through the center of the spindle axis (orange) and orthogonally crossing the crypt axis (yellow). Plane 2 is placed perpendicularly to plane 1 and parallel to the crypt long axis. (B) Angle determination. The left images show the top view of the cell in A to calculate α by projecting the crypt axis (yellow arrow) and spindle axis (orange line) on plane 1; large α angles contribute to crypt thickening. The right image shows the same cell viewed laterally to calculate β by projecting the crypt axis (yellow arrow) and spindle axis (orange line) on plane 2; large β angles lead to delamination of one daughter cell. Brown markings represent the apical junctional complex. (C) Optical section of intact colon crypts labeled for γ-tubulin (red), F-actin (green), and DNA (blue). The apical cell surface (arrow) shows a regular polygonal aspect. Mitotic cells (arrowheads) are positioned near the luminal side. Bar, 20 µm. (D) Isosurface rendering delineates the crypt lumen (green) defining its longitudinal axis (yellow line linking the two balls), the chromosomal masses (blue), and the spindle poles (red), which were used to determine the mitotic phase in which a cell was on fixation. (E and F) The values of α and β angles for colon crypts of wt ($Apc^{+/+}$), $Apc^{\Delta 14/+}$ (n = 45), $Apc^{1638N/+}$ (n = 52), and $Apc^{Min/+}$ (n = 47) mice, for SI crypts of $Apc^{Min/+}$ (n = 45) and colon ACF of $Apc^{\Delta 14/+}$ (n = 47) mice, and for colon crypts of floxed *Apc* × *Villin-CreERT2* mice treated with tamoxifen ($Apc^{-/-}$; n = 17). (G and H) Bar plots (top) and cumulative plots (bottom). The data show perturbation in both orientations in crypts of floxed *Apc* × *Villin-CreERT2* mice treated with tamoxifen, normal values in $Apc^{1638N/+}$, $Apc^{Min/+}$, and $Apc^{\Delta 14/+}$ mice (SI and colon) models, and significant perturbation of the longitudinal alignment, but normal planar alignment, in ACF of $Apc^{\Delta 14/+}$ mice.

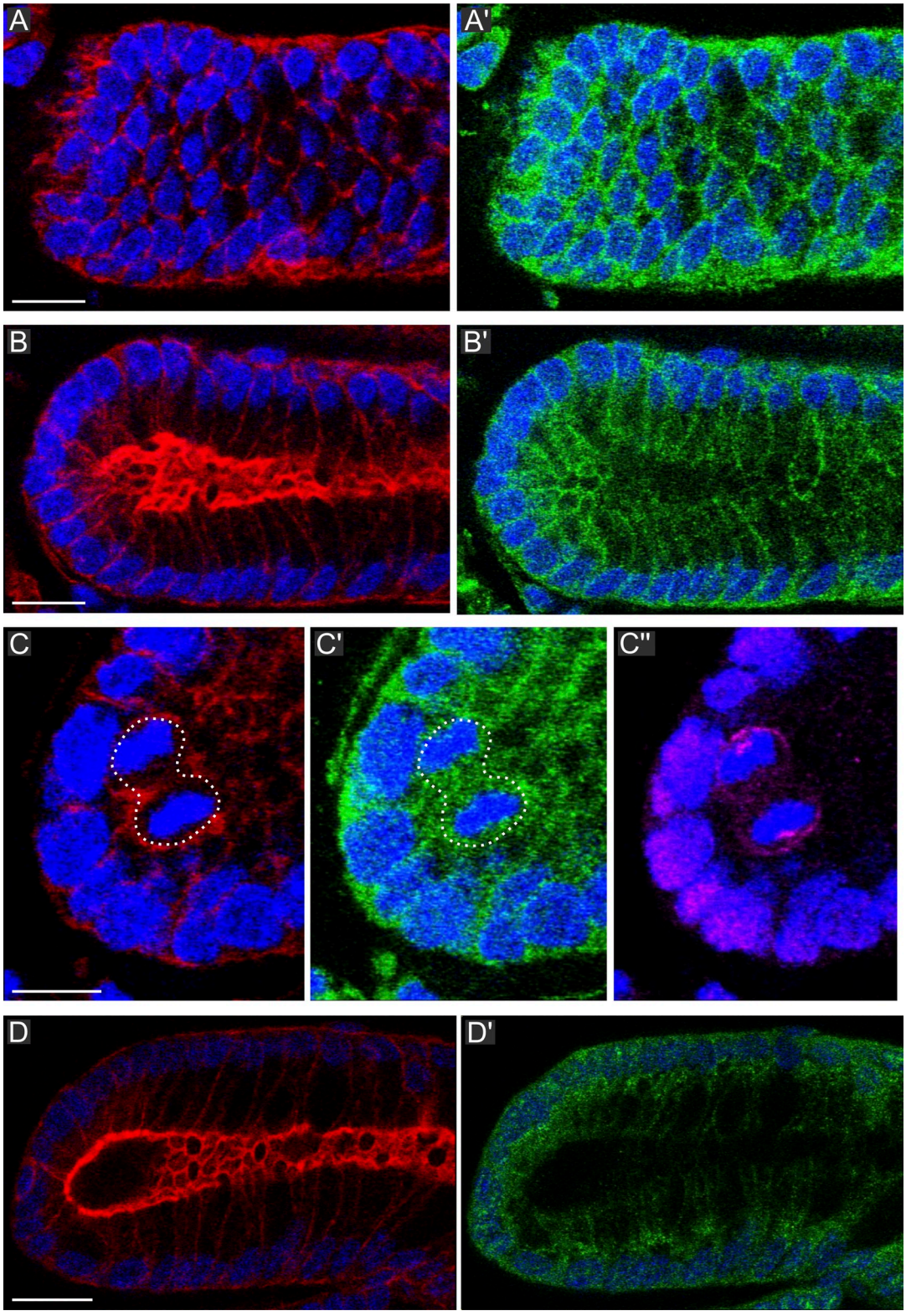

Figure S2. **Symmetric distribution of PCP proteins in colon crypts.** (blue) DAPI. A and A′ illustrate a parasagittal optical section of a wt crypt stained for actin (red; A) and for Celsr1 (green; A′). B and B′ illustrate a sagittal optical section of the same crypt stained for actin (B) and for Celsr1 (B′). Celsr1 is on cytoplasmic punctate structures and along the apicobasal membrane but absent from the apical poles. In A′, no polarization at the cortex along the crypt long axis can be detected. C–C′′ correspond to optical sections of a wt crypt passing through the poles of an early telophase cell at position 3 stained for actin (red; C), Celsr1 (green; C′), and NuMA (magenta; C′′). Note the absence of polarization at the cortex for Celsr1 and the cortical crescents near each pole for NuMA. The dotted lines delineate a cell of interest that is in telophase. D and D′ show a sagittal optical section of a wt crypt stained for actin (red; D) and for Vangl2 (green; D′). No polarization at the cortex along the crypt long axis can be detected. Bars: (A and B) 15 µm; (C) 10 µm; (D) 20 µm.

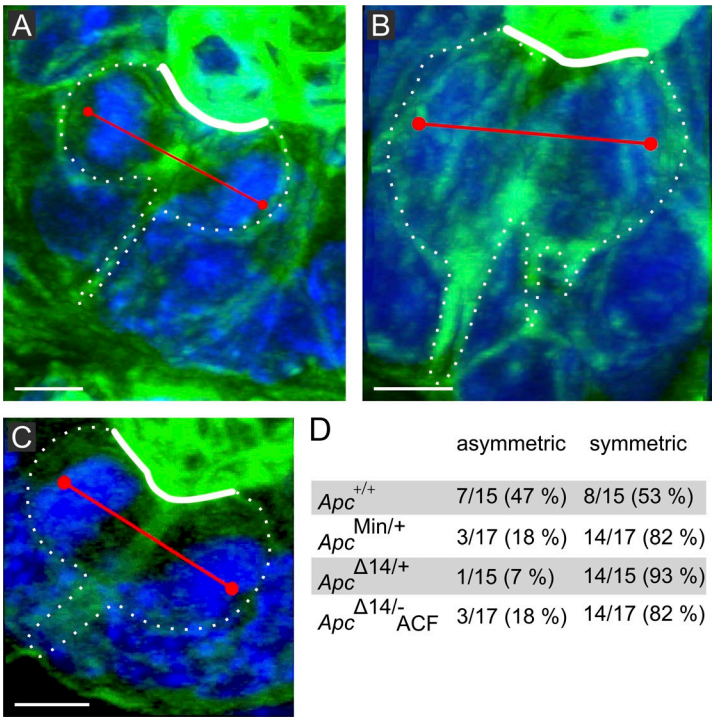

	asymmetric	symmetric
$Apc^{+/+}$	7/15 (47 %)	8/15 (53 %)
$Apc^{Min/+}$	3/17 (18 %)	14/17 (82 %)
$Apc^{\Delta 14/+}$	1/15 (7 %)	14/15 (93 %)
$Apc^{\Delta 14/-}$ ACF	3/17 (18 %)	14/17 (82 %)

Figure S3. **Inheritance of the BP in dividing cells of the crypt bottom.** (A and B) MIPs of telophases at the crypt base of wt mice show the BP linked to only one daughter cell (A) or to both daughters (B). Dotted lines show cell shape; white lines show apical surface; red lines show spindle axis. (C) Telophase in an $Apc^{Min/+}$ mouse exhibiting symmetric segregation of the BP. (D) Proportion of dividing cells showing asymmetric versus symmetric BP segregation in wt ($Apc^{+/+}$), $Apc^{Min/+}$, and $Apc^{\Delta 14/+}$ mice and in ACF ($Apc^{\Delta 14/-}$). Bars, 5 µm.

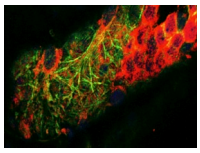

Video 1. **Animated optical sections through intact crypts flat mounted on a coverslip.** (green) F-actin; (blue) chromatin; (red) γ-tubulin. Note the good preservation of cytological details. A telophase is visible at the very bottom of the crypt. Fast confocal microscopy was used to collect image stacks. An acquisition typically consisted of 60 planes × 4 channels with a z step of 0.5 µm and a pixel size of 141 nm.

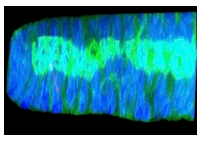

Video 2. **Animated MIPs tilt series of the optical sections through a crypt comprising a telophase at position 5 displaying a large (>80°) α angle.** (green) F-actin; (blue) chromatin; (red) a red line connecting the γ-tubulin–labeled spindle poles. Viewing 3D rotations of the F-actin signal combined with such a line allows visually determining spindle axis orientation with respect to crypt long axis orientation and the cleavage plane orientation with respect to the apical–basal cell polarity. Fast confocal microscopy was used to collect image stacks. An acquisition typically consisted of 60 planes × 4 channels with a z step of 0.5 µm and a pixel size of 141 nm. Using Imaris software, image stacks were processed for 3D mark positioning. For creating 3D rotations of a volume comprising a cell of interest, an image stack of a volume encompassing it was created using the Imaris 3D cropping function. Using the 3D measuring points function, a red line connecting the γ-tubulin–labeled spindle poles was incorporated into the stack.

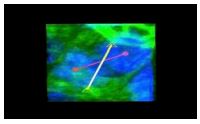

Video 3. **Animated MIPs tilt series of the cell in position 3 of the crypt in Fig. 1 A.** Depicted in Fig. 1 (C′ and C′′). (green) F-actin; (blue) chromatin; (red) a red line connecting the γ-tubulin–labeled spindle poles. Viewing 3D rotations of the F-actin signal combined with such a line allows visually determining spindle axis orientation with respect to crypt long axis orientation and the cleavage plane orientation with respect to the apical–basal cell polarity. Fast confocal microscopy was used to collect image stacks. An acquisition typically consisted of 60 planes × 4 channels with a z step of 0.5 µm and a pixel size of 141 nm. For creating 3D rotations of a volume comprising this cell, an image stack of a volume encompassing it was created using the Imaris 3D cropping function. Using the 3D measuring points function, a red line connecting the γ-tubulin–labeled spindle poles was incorporated into the stack.

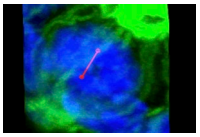

Video 4. **Animated MIP tilt series of the prometaphase in Fig. 1 D.** (green) F-actin; (blue) chromatin; (red) a red line connecting the γ-tubulin–labeled spindle poles. Viewing 3D rotations of the F-actin signal combined with such a line allows visually determining spindle axis orientation with respect to crypt long axis orientation and the cleavage plane orientation with respect to the apical–basal cell polarity. Fast confocal microscopy was used to collect image. An acquisition typically consisted of 60 planes × 4 channels with a z step of 0.5 µm and a pixel size of 141 nm. Using Imaris software, image stacks were processed for 3D mark positioning. For creating 3D rotations of a volume comprising this cell, an image stack of a volume encompassing it was created using the Imaris 3D cropping function. Using the 3D measuring points function, a red line connecting the γ-tubulin–labeled spindle poles was incorporated into the stack.

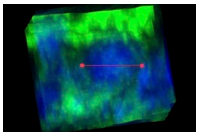

Video 5. **Animated MIP tilt series of a metaphase at position 5 after positioning it upright shows LOBA of a BP.** (green) F-actin; (blue) chromatin; (red) a red line connecting the γ-tubulin–labeled spindle poles. Viewing 3D rotations of the F-actin signal combined with such a line allows visually determining spindle axis orientation with respect to the apical–basal cell polarity and crypt long axis orientation. Fast confocal microscopy was used to collect image stacks An acquisition typically consisted of 60 planes × 4 channels with a z step of 0.5 µm and a pixel size of 141 nm. Using Imaris software, image stacks were processed for 3D mark positioning. For creating 3D rotations of a volume comprising this cell, an image stack of a volume encompassing it was created using the Imaris 3D cropping function. Using the 3D measuring points function, a red line connecting the γ-tubulin–labeled spindle poles was incorporated into the stack.

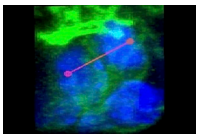

Video 6. **Animated MIP tilt series of the cell in Video 1.** (green) F-actin; (blue) chromatin; (red) a red line connecting the γ-tubulin–labeled spindle poles. Viewing 3D rotations of the F-actin signal combined with such a line allows determining visually spindle axis orientation with respect to crypt long axis orientation and the cleavage plane orientation with respect to the apical–basal cell polarity. Fast confocal microscopy was used to collect image stacks. An acquisition typically consisted of 60 planes × 4 channels with a z step of 0.5 µm and a pixel size of 141 nm. Using Imaris software, image stacks were processed for 3D mark positioning. For creating 3D rotations of a volume comprising this cell, an image stack of a volume encompassing it was created using the Imaris 3D cropping function. Using the 3D measuring points function, a red line connecting the γ-tubulin–labeled spindle poles was incorporated into the stack.

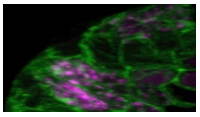

Video 7. **3D animation of the Atoh1$^{+/-}$ doublet sister cells in their environment.** Shown in Fig. 4 (C–C′′). (green) β-catenin; (red) Atoh1; (magenta) EdU; (blue) DAPI. One of the daughter cells of the EdU doublet at the bottom left (position 4–5) is clearly identifiable as Atoh1^{+}, and the other is identified as Atoh1^{-}.

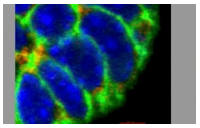

Video 8. **2D and 3D animation of the Atoh1$^{+/-}$ doublet sister cells in their environment.** Shown in Fig. 4 (D–D′′). (green) β-catenin; (red) Atoh1; (magenta) EdU; (blue) DAPI. The 2D animation allows tracing the signals through all the optical planes comprising the volume and identifying the nuclei that are Atoh1^{+}. The 3D animation shows the three doublet sister cells comprised in the volume. Marks were placed in the center of each nucleus and linked by a line, thus highlighting that they were located in different focal plains. Some Atoh1 labeling is present outside nuclei, but in the doublet at the crypt bottom (position 2–3), one nucleus is clearly identifiable as Atoh1^{+}, whereas the other is Atoh1^{-}. The same holds for the doublet to the right, which is sitting at another angle.

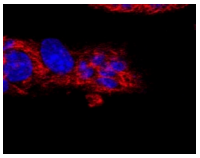

Video 9. **Animation of optical sections through a wt crypt containing a telophase at position 3.** Shown in Fig. 5 (A and B). (blue) DAPI; (red) actin; (green) mNumb; (magenta) NuMA. Fast confocal microscopy was used to collect image stacks. An acquisition typically consisted of 60 planes × 4 channels with a z step of 0.5 µm and a pixel size of 141 nm. The daughter cell closest to the crypt bottom is connected to the basal lamina through the basal process and displays a spot enriched in mNumb. Both daughter cells show cortical crescents of NuMA facing the centrosomes where NuMA labeling is strongest.

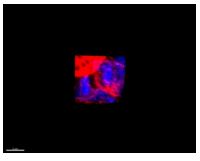

Video 10. **3D animation of the telophase shown in Fig. 5 (A and B) and Video 9.** (blue) DAPI; (red) actin; (green) mNumb. Fast confocal microscopy was used to collect the image. An acquisition typically consisted of 60 planes × 4 channels with a z step of 0.5 µm and a pixel size of 141 nm. For creating 3D rotations of a volume comprising this cell, an image stack of a volume encompassing it was created using the Imaris 3D cropping function. Viewing 3D rotations of the F-actin signal allows visualizing the BP linking one sister with the basal lamina. Well visible is that the daughter cell, in which mNumb is asymmetrically segregated, is also the one that is connected to the basal lamina by the BP.